Antiferromagnetic Blume-Capel model of the disordered Fe-Mn-Al ternary system

D. Peña Lara *

Grupo de Transiciones de Fases y Materiales Funcionales, Departamento de Física, Universidad del Valle, 760032, Cali, Colombia Centro de Excelencia en Nuevos Materiales (CENM), Universidad del Valle, Cali, Colombia

H. Correa

Laboratorio de Optoelectrónica, Universidad del Quindío, 630004, Armenia, Colombia

Daniel Suescún Díaz

Departamento de Física, Universidad Surcolombiana, 410001, Neiva, Colombia

(Received 11 April 2022; accepted 15 September 2022; published 12 October 2022)

The magnetic properties and thermodynamical description of the Fe-Mn-Al ternary alloy are studied using the spin 1 antiferromagnetic Blume-Capel (BC) model by the pair approximation based on the Gibbs-Feymann-Bogoliubov inequality for the free energy. The values of the spin operator are $+1$ for ferromagnetic interaction (Fe-Fe), -1 for the antiferromagnetic one (Mn-Mn, Mn-Fe), and 0 for the magnetic diluter (corresponding to Al). The BC model with antiferromagnetic (AF) next-nearest-neighbor coupling better accurately fit the mean hyperfine field experimental data obtained by Mössbauer spectroscopy. Considering the crystalline field, the predicted temperature as a function of the Al concentration phase diagram, for the fcc lattice, from the numerical solution is remarkably good and significantly improves the traditional Ising and random-site Ising models.

DOI: 10.1103/PhysRevE.106.044114

I. INTRODUCTION

Fe-Mn-Al ternary alloy is a lightweight stainless steel (SS) used to replace Fe-Cr-Ni-based SS due to its good mechanical properties [1,2], good corrosion resistance (inferior to SS) [3,4], wear-corrosion resistance, and improving oxidation resistance at high temperatures [5]. From the technological point of view, it has two applications: one is to use these mechanical properties at room temperature or high temperatures and the other is the diversity of its magnetic behaviors [6]. From the theoretical point of view, explaining those magnetic behaviors or phase transitions driven is by the manganese concentration, such as ferromagnetic $F \rightarrow$ paramagnetic P, spin-glass $SG \rightarrow P$, $AF \rightarrow P$, and so forth.

A phase diagram consists of phases in which a given macroscopic system can be found when specific thermodynamic parameters (temperature, pressure, concentration, among others) vary. Phase diagrams help optimize physical properties in alloys with specific compositions, develop new materials, control heat treatment procedures to produce specific properties, and so on. When the macroscopic system has three components it is called a ternary system.

This ternary alloy exhibits the α/γ phase equilibrium in the isotherm section at 1473 K (described by Köster and Torn [7]) and the β-manganese phase (discovered by Schmatz [8]) in the Fe-Mn-Al system with high manganese contents. In Murray's phase diagram, the γ phase is stable for the 20 wt pct Al and 50 wt pct Mn range, and the vast compositional space is the fcc phase. Chakrabarti [9], based on a metallographic method, confirmed the presence of the β-manganese phase and obtained the complete phase diagram using x-ray diffraction; however, above the 20 at pct Fe range, the body centered cubic (bcc) phase does not appear in the Mn-Al side in their results. Other phases have been found, such as α-Fe (bcc), β-Mn, γ-Fe (fcc), $FeAl_3$, and others. Many works about the experimental data of the Fe-Mn-Al system before 1983 were summarized by Rivlin [10].

The thermodynamic description in the Fe-Mn-Al system was reported in Refs. [11–13]. For this ternary system with magnetic ordering, the Gibbs energy is divided into two parts, one corresponding to no magnetic ordering and the other with magnetic ordering. The extensive regular solution model is used for a phase and the subregular solution model for the other phases. With the calculation of phase diagrams method (CALPHAD) [14,15], the experimental data reported in the literature are evaluated, obtaining a reasonable and self-consistent set of thermodynamic parameters to describe the system. The comparison between the calculated results and phase diagram information is in good agreement.

The Fe-Mn-Al alloy is a disordered system that presents a magnetic phase diagram with F, AF, P, SG, superparamagnetic (SP), and reentrant spin glass (RSG) phases. Pérez Alcázar *et al.*, with their experimental data, showed that this ternary alloy in the bcc and fcc phases depends on stoichiometry and thermal treatment [16–20]. Some competitive exchange interactions are as follows: an iron atom has a ferromagnetic competitive exchange interaction to their Fe first-neighbors ($J_{FeFe} > 0$), a manganese atom has an antiferromagnetic one both with Mn as Fe first-neighbors ($J_{MnMn} <$

*diego.pena@correounivalle.edu.co

0 and $J_{\mathrm{MnFe}} < 0$), and its nonmagnetic aluminum atom plays the role of a magnetic hole or single-site dilutor, characterizing this system as diluted.

Ising-like models were used to obtain the magnetic phase diagram as a function of temperature and concentration [21–24], taking into account two fundamental aspects: the random distribution of the elements and the competitivity in the first neighbor's interactions (ferromagnetic phase is for high Fe concentrations and the paramagnetic one for low Fe concentrations). Although the Ising-like model fits the reduced mean hyperfine field as a function of Mn, Al, and Fe concentration experimental data, subtle differences are evident. Both Al and Mn atoms serve as dilutors. For the respective magnetic phase diagram, the fittings from the ferromagnetic phase to the paramagnetic one are well; however, the results are not as expected when the transition is from the AF phase to the P phase. The reason not considered in the Ising model is that the Fe-Mn-Al system shows magnetic anisotropy.

The magnetic anisotropy present in the ternary alloy will be considered using the AF Blume [25] and Capel model [26] (BC), which introduces the crystal field concept in the iron group ions whose electronic configuration is $3d$. With this BC model introduced to study the ternary Fe-Ni-Mn and Fe-Al-Mn alloys [27,28], the reduced mean hyperfine field is a function of Mn, Al, and Fe concentration and the phase diagram is in much better accord with the experimental data.

In this work, we fit the experimental data of the reduced mean hyperfine field as a function of Al concentration at room temperature and the phase diagram of temperature as a function of Mn concentration of this disordered magnetic ternary alloy using the AF BC model by pair approximation introduced by Ferreira *et al.* [29].

II. ANTIFERROMAGNETIC BLUME-CAPEL MODEL AND PAIR APPROXIMATION

The AF three-state BC model [25,26] $\sigma = 1$ is given by the following Hamiltonian:

$$\mathcal{H}_{\mathrm{BC}}(\sigma_i, \Delta_i) = -\sum_{\langle ij \rangle} J_{ij}\sigma_i\sigma_j + \sum_i \Delta_i\sigma_i^2, \tag{1}$$

where the first sum runs over all first neighbor pairs of interacting sites i and j for N lattice sites. Here, the negative site-dependent bilinear exchange interaction parameter between the nearest-neighbors spins ($J_{ij} < 0$) defines the AF BC model; σ_i are the spins with values -1, 0, 1; and $\Delta_i = \Delta$ is the single-spin anisotropy parameter (also called the crystal field). Δ describes the electrostatic interactions between a metal ion and ligands (represented as negative charges) in the crystal.

The Hamiltonian (1) introduced by Blume [25] and Capel [26] independently has two quantities, namely, the mean magnetization m and the mean quadrupole moment Q:

$$m = \langle\sigma_i\rangle; \quad Q = \langle\sigma_i^2\rangle, \tag{2}$$

and it can be applied to describe various systems as multicomponent fluids [30], magnetic systems (in the context of tricritical phenomena) [31,32], nanowire [33], as well as ternary alloys [27,28].

As the Hamiltonian (1) has no exact solution for dimensions greater than 1, many schemes such as the mean-field approximation [34,35], Monte Carlo simulations [36,37], mean-field renormalization group (MFRG) method [38,39], and position-space renormalization-group methods [40] among others, were widely used.

The AF BC model has been studied widely. The transfer matrix technique studied the magnetocaloric properties, specific heat, and ground-state phase diagram [41]. By mean-field theory, in the presence of a uniform external magnetic field, the phase diagram exhibits reentrant behavior and tricritical, bicritical, and triple points [42]. Other authors performed Monte Carlo simulations on a triangular lattice using the Wang-Landau sampling method showing the critical lines and their phase diagrams [43].

The exchange coupling for this disordered system is to consider the following probability distribution $P(J_{ij})$:

$$\begin{aligned} P(J_{ij}) = {} & p^2\delta(J_{ij} - J) + x^2\delta(J_{ij} + \alpha J) \\ & + 2px\delta(J_{ij} + \gamma J) + q(2-q)\delta(J_{ij}), \end{aligned} \tag{3}$$

where p^2 is the probability of having two Fe atoms with interaction J, x^2 the probability of having two Mn atoms with interaction $-\alpha J$, $2px$ the probability of having a couple of FeMn atoms with interaction $-\gamma J$, and $q(2-q)$ represents all the nonmagnetic bonds with Al atoms (FeAl, MnAl, and AlAl) given by $q^2 + 2qp + 2qx = q(2-q)$. Here p, x, q are the concentrations of Fe, Mn, Al, respectively (with the condition $p + q + x = 1$), α and γ are the parameters to adjust.

We will study the spin $\sigma = 1$ Blume-Capel model given by the Hamiltonian (1), considering insulated single spins and linked pairs. The variational principle for the free energy based on the Gibbs-Feymann-Bogoliubov inequality [44] is applied following the procedure in Ref. [29]

$$\begin{aligned} F\left(\gamma_s^i, \Gamma_s^i; \gamma_p^i, \Gamma_p^i\right) \leqslant {} & \left[F_0\left(\gamma_s^i, \Gamma_s^i; \gamma_p^i, \Gamma_p^i\right)\right] \\ & + \left[\langle\mathcal{H} - \mathcal{H}_0\left(\gamma_s^i, \Gamma_s^i; \gamma_p^i, \Gamma_p^i\right)\rangle_0\right], \end{aligned} \tag{4}$$

where F is the $\mathcal{H}$ Hamiltonian free energy given by (1), $F_0(\gamma_s^i, \Gamma_s^i; \gamma_p^i, \Gamma_p^i)$ is the trial $\mathcal{H}_0$ Hamiltonian (conveniently parametrized), i means the sublattices a and b, $\langle\cdots\rangle_0$ indicates the thermal average on an assembly defined by $\mathcal{H}_0$, and $[\cdots]$ denotes the configurational average according to the probability distribution (3). For this case, the $\mathcal{H}_0$ Hamiltonian is

$$\mathcal{H}_0 = \sum_{\mathrm{is}} \mathcal{H}_s^i + \sum_{\mathrm{ps}} \mathcal{H}_p^i, \tag{5}$$

with $\mathcal{H}_s$ being the isolated single spin Hamiltonian, given by

$$\mathcal{H}_s = -\gamma_{\mathbf{s}}^{\mathbf{a}}\sigma_a - \gamma_{\mathbf{s}}^{\mathbf{b}}\sigma_b - \mathbf{\Gamma}_{\mathbf{s}}^{\mathbf{a}}\sigma_a^2 - \mathbf{\Gamma}_{\mathbf{s}}^{\mathbf{b}}\sigma_b^2 + \Delta\left(\sigma_a^2 + \sigma_b^2\right), \tag{6}$$

and $\mathcal{H}_p$ the linked pairs of spins Hamiltonian given by

$$\begin{aligned} \mathcal{H}_p = {} & -J_{ij}\sigma_a\sigma_b - \gamma_{\mathbf{p}}^{\mathbf{a}}\sigma_a - \mathbf{\Gamma}_{\mathbf{p}}^{\mathbf{a}}\sigma_a^2 - \gamma_{\mathbf{p}}^{\mathbf{b}}\sigma_b \\ & - \mathbf{\Gamma}_{\mathbf{p}}^{\mathbf{b}}\sigma_b^2 + \Delta\left(\sigma_a^2 + \sigma_b^2\right). \end{aligned} \tag{7}$$

The first sum in (5) runs over the $N - 2n$ isolated spins (is) and the second one over the n pairs of disconnected spins (ps), with N being the total amount of spins. The variational parameters γ_s^i, Γ_s^i, γ_p^i y Γ_p^i are determined by using the minimization condition for the free energy [29].

In this case, the free energy F_0 is

$$f_0 \equiv -\frac{\beta F_0}{N} = \{\ln[\mathrm{Tr}(\rho_0)]\}$$
$$= \left[\frac{z}{2}\ln[Tr(\rho_p)] + (1-z)\ln[\mathrm{Tr}(\rho_s)] + (1-z)\left\{\gamma_s^i\langle\sigma\rangle_0 + \Gamma_s^i\langle\sigma^2\rangle_0\right\} + z\left\{\gamma_p^i\langle\sigma\rangle_0 + \Gamma_p^i\langle\sigma^2\rangle_0\right\}\right], \quad (8)$$

where Tr is the trace of the density matrix ρ, z is the lattice coordination number, and ρ_s and ρ_p are the density matrices for a single isolated spin and linked pairs of spins Hamiltonians, respectively. These matrices are given by

$$\rho_s = \exp(-\beta\mathcal{H}_s), \quad (9)$$

$$\rho_p = \exp(-\beta\mathcal{H}_p). \quad (10)$$

Now it is assumed that the mean values $m = \langle\sigma\rangle$ and $q = \langle\sigma^2\rangle$ are obtained from $\mathcal{H}_s$ and $\mathcal{H}_p$, this is

$$m\left(\gamma_s^i, \Gamma_s^i\right) = [\mathrm{Tr}(\rho_s\langle\sigma\rangle)] = \left[\tfrac{1}{2}\mathrm{Tr}(\rho_p\langle\sigma\rangle)\right], \quad (11)$$

$$Q\left(\gamma_p^i, \Gamma_p^i\right) = [\mathrm{Tr}(\rho_s\langle\sigma^2\rangle)] = \tfrac{1}{2}\left[\mathrm{Tr}(\rho_p\langle\sigma^2\rangle)\right]. \quad (12)$$

The minimization of (8) as a function of the variational parameters γ_s^i, Γ_s^i, γ_p^i y Γ_p^i, taking $n = Nz/2$ [39] drives us to the following relations:

$$(z-1)\gamma_s^i = z\gamma_p^i, \quad (z-1)\Gamma_s^i = z\Gamma_p^i. \quad (13)$$

The set of Eqs. (11) to (13) presents several solutions for the order parameter m, which must be done under the numerical method to obtain the second-order transition lines in the phase diagram.

III. APPLICATION TO THE FE-MN-AL TERNARY SYSTEM

The Fe-Mn-Al ternary system in its face centered cubic (fcc)-disordered phase is AF; therefore, to study it, we have to divide the loose-packed lattice into two sublattices a and b, with each one having as magnetization m_A and m_B, respectively. The expressions for these magnetizations are given in the Appendix; see Eqs. (A3) and (A4). For our case, we interpret the spin variables as the zero-state corresponds to the magnetic diluter, the $+1$ state is for the ferromagnetic interaction (Fe-Fe), and the -1-state for the antiferromagnetic one (Mn-Mn, Mn-Fe).

After performing the configurational averages, two transcendental equations (present in the Appendix), one for the magnetization and the other for the quadrupole moment, must be solved by numerical methods. Using the FINDROOT function of the MATHEMATICA software, the roots of these pairs of equations are obtained.

Using the probability distribution (3), we note that J_{ij} takes values randomly according to our model's interpretation. The lattice parameter increases linearly by increasing the Al concentration q in this disordered system. Therefore, the exchange parameter J as a function of q is a decreased function [45]. Thus we can assume that

$$J(q) = J_1 - qJ_0, \quad (14)$$

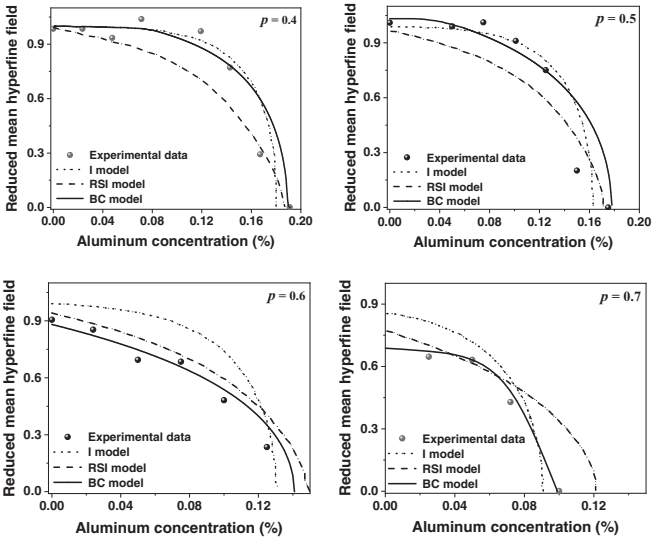

FIG. 1. The reduced mean hyperfine field $\bar{H}$ behavior as a function of Al concentration q for a fixed Fe concentration (a) $p = 0.4$, (b) $p = 0.5$, (c) $p = 0.6$, and (d) $p = 0.7$. The full circles represent experimental data; the dotted and dashed lines are the theoretical fittings from the traditional Ising and random-site Ising models. The data are from Ref. [46]. The solid line is the solution of Eq. (14) whose parameters are in the text.

with J_1 and J_0 being the adjusted parameters with values $J_1 = 15.3$ meV and $J_0 = 2.81J_1$ meV.

IV. RESULTS

The experimental data cited by the authors of Ref. [46] of the reduced mean hyperfine field as a function of aluminum concentration q for various fixed iron concentrations p at room temperature were obtained by Mössbauer spectroscopy.

The behavior for $p = 0.4, 0.5, 0.6$, and 0.7 for the Fe-Mn-Al ternary system, in Figs. 1(a), 1(b), 1(c), and 1(d) are displayed, respectively. The dotted line is the fitting using the traditional Ising model, the dashed line corresponds to the random-site Ising (RSI) model [46], and the solid line is obtained using the AF BC model.

For the traditional Ising model, the role assumed by the magnetic dilutor is to take into account that the sum of their spins gives zero ($\sigma_{+1} + \sigma_{-1} = 0$); in other words, the interactions among Al atoms with Fe and Mn atoms would be zero. For the random-site Ising model from Ref. [46], the authors assumed that Al atoms have no magnetic moment and serve as a single-site dilutor. This fact, illustrated by the authors, reflected the choice of the interactions among Al atoms with Fe and Mn atoms as null ($J_{\mathrm{AlFe}} = 0 = J_{\mathrm{AlMn}}$). For the AF BC model, their three states corresponded to the natural different interactions present in the system: σ_{-1}, σ_0, and σ_{+1} would be the interactions among J_{FeMn}, J_{AlMn} and J_{AlFe}, and J_{MnMn}, respectively. The solid line passes equitably through the experimental data better than the Ising and RSI models; some experimental data are out of the fitting line.

In Fig. 1(a), both the AF BC and RSI models fit all the experimental data reported in Ref. [46] while in the Ising

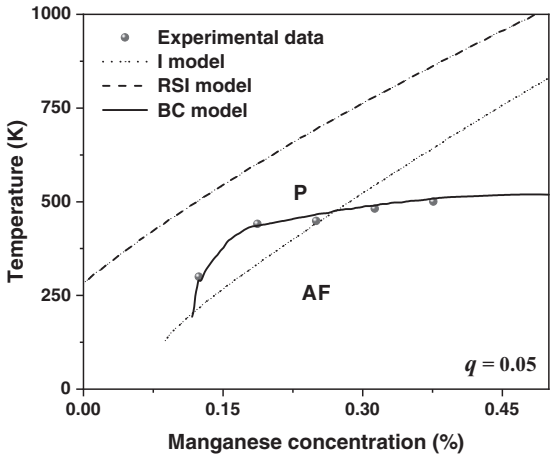

FIG. 2. Temperature as a function of Mn concentration (x) for a fixed Al concentration $q = 0.05$. The full circles are the experimental data from Ref. [46], the dotted line corresponds to the theoretical fitting from the traditional Ising model, the dashed line is the fitting using random-site Ising model from Ref. [46]. The solid line is from the present AF BC model.

model the fit is only for the first three and the last two points, but the behavior is far from the experimental data.

In Fig. 1(b), the three-curve fits show similar behavior to that obtained in Fig. 1(a). The curve fitted by the AF BC model is better than the one predicted by the RSI model. The Ising model fits only the first and last experimental data.

In Fig. 1(c), the Ising model only fits the last point of the experimental data, the fittings curve of the RIS model is above the experimental data, and the AF BC model, on average, fits the wentire behavior.

In Fig. 1(d), the Ising and RMI models do not fit all of the behavior of the reduced hyperfine field as a function of aluminum concentration. The fit to the experimental data using the present model is good.

The software used to resolve the numerical solutions was MATHEMATICA. The value for the single-spin anisotropy parameter was 2.5 meV and equal to all concentrations fitted.

Figure 2 shows the behavior of temperature as a function of Mn concentration x in the range 0 to 0.5 for a fixed aluminium concentration $q = 0.05$. The black dots correspond to the experimental data [1], the dotted line is the fit using the traditional Ising model, the dashed line for the random site Ising model, and the solid line is the predicted curve using the AF BC model. The expected behavior for the Ising and RSI models is similar, however, the predicted curve is far from the experimental data. The fit is outstanding, considering the magnetic anisotropy and the three independent states for the AF BC model.

V. CONCLUSION AND REMARKS

Comparing the antiferromagnetic Blume-Capel model with the traditional Ising model and the random site Ising model, the fits achieved are very good. The AF BC model fits much better than those that do not consider the anisotropy parameter or the crystal field. We observe that when p increases, the fit of the AF BC model improves. The fits are more accurate for iron concentration $p = 0.7$, as shown in Fig. 1.

The prediction of the temperature as a function of the %Mn phase diagram from the numerical solution is remarkably good and significantly improved regarding the traditional Ising and random-site Ising models. The same happened for predicting the temperature versus the %Mn phase diagram for the $(Fe_{0.65}Ni_{0.35})_{1-x}Mn_x$ system [27].

APPENDIX

In this Appendix, we present the two transcendental equations using the expectation value of any observable $\mathcal{O}$

$$\langle\widehat{\mathcal{O}}\rangle = \int_{\langle J_{ij}\rangle} P(J_{ij})\mathcal{O}\, dJ_{ij}, \tag{A1}$$

where J_{ij} is the random-bond distribution (3).

In what follows we have

$$r = \frac{z-1}{z}, \qquad d = \beta\Delta, \qquad K = \beta J,$$
$$v = \beta\gamma_s^a, \qquad u = \beta\gamma_s^b, \qquad V = \beta\Gamma_s^a,$$
$$U = \beta\Gamma_s^b, \qquad A = e^{U-d}, \qquad B = e^{V-d}.$$

The partition function for the isolated spins is

$$Z_s = 1 + 2B\cosh(v) + 2A\cosh(u) + 4AB\cosh(v)\cosh(u). \tag{A2}$$

The magnetization for the isolated spins is as follows:

$$m_s^a = \frac{B\sinh(v)[1 + 2A\cosh(u)]}{Z_s}, \tag{A3}$$
$$m_s^b = \frac{A\sinh(u)[1 + 2B\cosh(v)]}{Z_s}. \tag{A4}$$

The quadrupole for the isolated spins is

$$Q_s^a = \frac{B\cosh(v)[1 + 2A\cosh(u)]}{Z_s}, \tag{A5}$$
$$Q_s^b = \frac{A\cosh(u)[1 + 2B\cosh(v)]}{Z_s}. \tag{A6}$$

The partition function for the pairs of disconnected spins is

$$Z_{pp} = 1 + 2e^{rv-d}\cosh(r\,v) + 2e^{rU-d}\cosh(r\,u) + 2e^{r(V+U)+K-2d}\cosh[r(v+u)] + 2e^{r(V+U)-K-2d}\cosh[r(v-u)], \tag{A7}$$

$$Z_{px} = 1 + 2e^{rV-d}\cosh(r\,v) + 2e^{rU-d}\cosh(r\,u) + 2e^{r(V+U)-\alpha K-2d}\cosh[r(v+u)] + 2e^{r(V+U)+\alpha K-2d}\cosh[r(v-u)],$$
$$Z_{ppx} = 1 + 2e^{rV-d}\cosh(r\,v) + 2e^{rU-d}\cosh(r\,u) + 2e^{r(V+U)-\gamma K-2d}\cosh[r(v+u)] + 2e^{r(V+U)+\gamma K-2d}\cosh[r(v-u)], \tag{A8}$$

$$Z_{pq} = 1 + 2e^{rV-d}\cosh(r\,v) + 2e^{r\,U-d}\cosh(r\,u) + 2e^{r(V+U)-2d}\cosh[r(v+u)] + 2e^{r(V+U)-2d}\cosh[r(v-u)]. \tag{A9}$$

The magnetization for the pairs of disconnected spins is as follows:

$$\begin{aligned} m_p^a = {} & \frac{p^2}{Z_{pp}}(e^{r(V+U)+K-2d}\sinh[r(v+u)] + e^{r(V+U)-K-2d}\sinh[r(v-u)] + e^{r\,V-d}\sinh(r\,v)) \\ & + \frac{x^2}{Z_{px}}(e^{r(V+U)-\alpha K-2d}\sinh[r(v+u)] + e^{r(V+U)+\alpha K-2d}\sinh[r(v-u)] + e^{r\,V-d}\sinh(r\,v)) \\ & + \frac{2px}{Z_{ppx}}(e^{r(V+U)-\gamma K-2d}\sinh[r(v+u)] + e^{r(V+U)+\gamma K-2d}\sinh[r(v-u)] + e^{r\,V-d}\sinh(r\,v)) \\ & + \frac{q(2-q)}{Z_{pq}}(e^{r(V+U)-2d}\sinh[r(v+u)] + e^{r(V+U)-2d}\sinh[r(v-u)] + e^{r\,V-d}\sinh(r\,v)), \end{aligned}$$

$$\begin{aligned} m_p^b = {} & \frac{p^2}{Z_{pp}}(e^{r(V+U)+K-2d}\sinh[r(v+u)] - e^{r(V+U)-K-2d}\sinh[r(v-u)] + e^{r\,U-d}\sinh(r\,u)) \\ & + \frac{x^2}{Z_{px}}(e^{r(V+U)-\alpha K-2d}\sinh[r(v+u)] - e^{r(V+U)+\alpha K-2d}\sinh[r(v-u)] + e^{r\,U-d}\sinh(r\,u)) \\ & + \frac{2px}{Z_{ppx}}(e^{r(V+U)-\gamma K-2d}\sinh[r(v+u)] - e^{r(V+U)+\gamma K-2d}\sinh[r(v-u)] + e^{r\,U-d}\sinh(r\,u)) \\ & + \frac{q(2-q)}{Z_{pq}}(e^{r(V+U)-2d}\sinh[r(v+u)] - e^{r(V+U)-2d}\sinh[r(v-u)] + e^{r\,U-d}\sinh(r\,u)). \end{aligned}$$

The quadrupole for the pairs of disconnected spins is

$$\begin{aligned} Q_p^a = {} & \frac{p^2}{Z_{pp}}(e^{r(V+U)+K-2d}\cosh[r(v+u)] + e^{r(V+U)-K-2d}\cosh[r(v-u)] + e^{r\,V-d}\cosh(r\,v)) \\ & + \frac{x^2}{Z_{px}}(e^{r(V+U)-\alpha K-2d}\cosh[r(v+u)] + e^{r(V+U)+\alpha K-2d}\cosh[r(v-u)] + e^{r\,V-d}\cosh(r\,v)) \\ & + \frac{2px}{Z_{ppx}}(e^{r(V+U)-\gamma K-2d}\cosh[r(v+u)] + e^{r(V+U)+\gamma K-2d}\cosh[r(v-u)] + e^{r\,V-d}\cosh(r\,v)) \\ & + \frac{q(2-q)}{Z_{pq}}(e^{r(V+U)-2d}\cosh[r(v+u)] + e^{r(V+U)-2d}\cosh[r(v-u)] + e^{r\,V-d}\cosh(r\,v)), \end{aligned}$$

$$\begin{aligned} Q_p^b = {} & \frac{p^2}{Z_{pp}}(e^{r(V+U)+K-2d}\cosh[r(v+u)] + e^{r(V+U)-K-2d}\cosh[r(v-u)] + e^{r\,U-d}\cosh(r\,u)) \\ & + \frac{x^2}{Z_{px}}(e^{r(V+U)-\alpha K-2d}\cosh[r(v+u)] + e^{r(V+U)+\alpha K-2d}\cosh[r(v-u)] + e^{r\,U-d}\cosh(r\,u)) \\ & + \frac{2px}{Z_{ppx}}(e^{r(V+U)-\gamma K-2d}\cosh[r(v+u)] + e^{r(V+U)+\gamma K-2d}\cosh[r(v-u)] + e^{r\,U-d}\cosh(r\,u)) \\ & + \frac{q(2-q)}{Z_{pq}}(e^{r(V+U)-2d}\cosh[r(v+u)] + e^{r(V+U)-2d}\cosh[r(v-u)] + e^{r\,U-d}\cosh(r\,u)). \end{aligned}$$

[1] K. Chung, K. Ahn, D. H. Yoo, K. H. Chung, M. H. Seo, and S. H. Park, Int. J. Plast. **27**, 52 (2011).

[2] G. A. Pérez Alcázar, Rev. Acad. Colomb. Cienc. **28**, 265 (2004).

[3] F.-Q. Yang, R. B. Song, L. F. Zhang, and C. Zhao, Procedia Eng. **81**, 456 (2014).

[4] H.-H. Huang and T.-H. Chuang, Materials Science and Engineering: A **292**, 90 (2000).

[5] Y. H. Guu and M. T.-K. Hou, Materials Science and Engineering: A **466**, 61 (2007).

[6] J. D. Betancur-Ríos, K. Nomura, G. A. Pérez Alcázar, and J. A. Tabares, Hyperfine Interact. **187**, 43 (2008).

[7] W. Köster and W. Torn, Arch. Eisenhüttenwes **7**, 365 (1933).
[8] D. J. Schmatz, Trans. ASM **52**, 898 (1960).
[9] D. J. Chakrabarti, Metall. Trans. B **8**, 121 (1977).
[10] V. G. Rivlin, Int. Metals Rev. **28**, 309 (2013).
[11] L. Xingjun and H. Shiming, Calphad **17**, 79 (1993).
[12] L.-H. Zhou, Z. Li, S.-S. Wang, R.-M. Hu, S.-H. Wang, Z.-W. Qin, X.-G. Lu, and C.-H. Li, Adv. Manuf. **6**, 247 (2018).
[13] M.-S. Kim and Y.-B. Kang, J. Phase Equilib. Diffus. **36**, 453 (2015).
[14] A. K. Mallik, Bull. Mater. Sci. **8**, 107 (1986).
[15] L. Kaufman and H. Bernstein, *Computer Calculation of Phase Diagrams* (Academic, New York, 1970).
[16] G. A. Pérez Alcázar, J. A. Plascak, and E. Galvão da Silva, Phys. Rev. B **38**, 2816 (1988).
[17] G. A. Pérez Alcázar, E. Galvão da Silva, and C. Paduani, Hyperfine Interact. **66**, 221 (1991).
[18] J. Restrepo, G. A. Pérez Alcázar, and J. M. Gónzalez, J. Appl. Phys. **87**, 7425 (2000).
[19] M. M. Rico Castro, M. H. Medina Barreto, and G. A. Pérez Alcázar, Hyp. Interac. **128**, 503 (2000).
[20] G. A. Pérez Alcázar, C. González, and B. Cruz, Hyperfine Interact. **148**, 295 (2003).
[21] J. Restrepo and G. A. Pérez Alcázar, Phys. Rev. B **61**, 5880 (2000).
[22] L. E. Zamora, G. A. Pérez Alcázar, C. González, J. M. Greneche, W. R. Aguirre, A. Bohórquez, E. M. B. Saitovich, and D. Sánchez, J. Magn. Magn. Mater. **301**, 495 (2006).
[23] E. A. Velásquez, L. F. Duque, J. Mazo-Zuluaga, and J. Restrepo, Phys. B: Condens. Matter **398**, 364 (2007).
[24] H. Zhang, S. Lu, M. Zhou, M. P. J. Punkkinen, B. Johansson, and L. Vitos, J. Appl. Phys. **118**, 103904 (2015).
[25] M. Blume, Phys. Rev. **141**, 517 (1966).
[26] H. W. Capel, Physica **32**, 966 (1966).
[27] D. Peña Lara, G. A. Pérez Alcázar, L. E. Zamora, and J. A. Plascak, Phys. Rev. B **80**, 014427 (2009).
[28] D. Peña Lara, J. E. Diosa, and C. A. Lozano, Phys. Rev. E **87**, 032108 (2013).
[29] L. G. Ferreira, S. R. Salinas, and M. J. Oliveira, Phys. Stat. Sol. (B) **83**, 229 (1977).
[30] D. Mukamel and M. Blume, Phys. Rev. A **10**, 610 (1974).
[31] N. G. Fytas, J. Zierenberg, P. E. Theodorakis, M. Weigel, W. Janke, and A. Malakis, Phys. Rev. E **97**, 040102(R) (2018).
[32] J. D. Kimel, P. A. Rikvold, and Y.-L. Wang, Phys. Rev. B **45**, 7237 (1992).
[33] H. Magoussi, A. Zaim, and M. Kerouad, Solid State Commun. **200**, 32 (2014).
[34] J. A. Plascak, J. G. Moreira, and F. C. sá Barreto, Phys. Lett. A **173**, 360 (1993).
[35] P. V. Santos, F. A. da Costa, and J. M. de Araújo, Phys. Lett. A **379**, 1397 (2015).
[36] C. J. Silva, A. A. Caparica, and J. A. Plascak, Phys. Rev. E **73**, 036702 (2006).
[37] M. Hasenbusch, Phys. Rev. E **101**, 022126 (2020).
[38] D. Peña Lara and J. A. Plascak, Mod. Phys. Lett. B **10**, 1067 (1996).
[39] D. Peña Lara and J. A. Plascak, Int. J. Mod. Phys. B **12**, 2045 (1998).
[40] G. D. Mahan and S. M. Girvin, Phys. Rev. B **17**, 4411 (1978).
[41] Y.-P. Guo, Z.-Q. Liu, Y.-L. Xu, and X.-M. Kong, Phys. Rev. E **93**, 052151 (2016).
[42] K. Argın and O. Canko, Physica A **391**, 2556 (2012).
[43] S. Park and W. Kwak, J. Phys.: Conf. Series **738**, 012126 (2016).
[44] Z.-G. Wang, *Variational Methods in Molecular Modeling*, edited by J. Wu (Springer Singapore, Singapore, 2017), pp. 1–29.
[45] G. A. Pérez Alcázar, J. A. Plascak, and E. Galvão da Silva, Phys. Rev. B **34**, 1940 (1986).
[46] A. Osorio, W. R. Aguirre Contreras, L. E. Zamora, G. A. Pérez Alcazar, and J. A. Plascak, Phys. Rev. B **68**, 024420 (2003).